Lawrence Berkeley Laboratory
UNIVERSITY OF CALIFORNIA

ENERGY & ENVIRONMENT DIVISION

Submitted to the Journal of Applied Physics

PIEZOELECTRIC PHOTOACOUSTIC DETECTION: THEORY & EXPERIMENT

Warren Jackson and Nabil M. Amer

October 1979

Prepared for the U.S. Department of Energy under Contract W-7405-ENG-48

DISCLAIMER

PIEZOELECTRIC PHOTOACOUSTIC DETECTION: THEORY & EXPERIMENT

Warren Jackson

Nabil M. Amer

Applied Laser Spectroscopy Group

Lawrence Berkeley Laboratory

University of California

Berkeley, California 94720

(Received

ABSTRACT

The theory of piezoelectric photoacoustic spectroscopy is developed for condensed matter samples. The three-dimensional thermoelastic equations are solved for a layer using a Green's function for the stress. Expressions for the dependence of the signal on absorption, modulation frequency, thermal properties, and mechanical properties of the sample are derived. The theoretical predictions are experimentally verified, the sources of noise are analyzed and the noise equivalent power (NEP) is estimated. Finally, considerations for detector optimization are discussed.

PACS numbers: 07.60.-j,07.65.-b,78.20.-e

PIEZOELECTRIC PHOTOACOUSTIC DETECTION: THEORY & EXPERIMENT

Warren Jackson

Nabil M. Amer

Applied Laser Spectroscopy Group

Lawrence Berkeley Laboratory

University of California

Berkeley, California 94720

(Received

I. INTRODUCTION

When an intensity modulated light beam is absorbed by a medium, part or all of the excitation energy is converted to thermal energy. In "conventional" photoacoustic spectroscopy, the generated heat is coupled to an optically nonabsorbing gas and the time-dependent pressure fluctuation is detected with a microphone. The universal applicability of this approach to gases,[1-6] liquids,[7-9] solids,[10-14] and aerosols[15,16] makes it a versatile detector scheme. Nevertheless, this approach suffers from certain crucial limitations, particularly in the case of condensed matter samples. Perhaps the most serious restrictions are the narrow bandwidth of the microphone response, the relatively complex nature of the heat transfer process from the sample to the gas, and the inability to perform experiments at low pressures. Furthermore, saturation problems limit the usefulness of this technique in the case of

strong optical absorption.

Recently, an alternative photoacoustic scheme has been developed utilizing a piezoelectric transducer (PZT) attached directly to the sample.[17-20] The absorption-induced heating causes the sample to develop thermal stresses and strains which are transmitted to the sample surface. A PZT attached to the sample converts these stresses and strains to a measurable voltage.

This approach has several advantages over gas cell photoacoustics. PZT's have a wide frequency response range from a few Hz to many MHz, and they can be employed over a broad range of temperatures and pressures. Since the sample-PZT configuration is compact and rugged, it is useful in space-limited experiments (e.g., inside a low temperature optical dewar). Because the PZT responds to absorption of radiation by the entire sample, not merely within a thin thermal length, the complicated solid-gas coupling is eliminated. Furthermore, as we shall demonstrate, piezoelectric-photoacoustic spectroscopy (PZT-PAS) is a very sensitive means for measuring absorption coefficients as low as 10^{-5} cm^{-1} for a 1 W laser, and does not show saturation for $\alpha\ell$ as high as 10.

Until now there has been a few attempts to develop a theoretical model for the piezoelectric signal or to compare its predictions with experiments[19,21]. In order to simplify calculations, previous theories have assumed that the absorption of the sample is very small and that the sample is a long cylinder. However, the samples often have significant absorption and cannot be conveniently made into cylindrical shapes. Furthermore, the cylindrical geometry does not minimize the scattering of light onto the transducer as well as other geometries would.

Finally, there are discrepancies between theory and experiment which have not been satisfactorily explained[19].

In this paper we develop a computationally tractable thermoelastic theory for piezoelectric photoacoustic detection at low modulation frequencies. This theory was tested experimentally with samples whose thermal and optical properties cover a wide range. We find that our theoretical treatment quantitatively accounts for the observed magnitude and phase of the signal, and describes its functional dependence on modulation frequency, absorption coefficients, and thermal properties of the sample.

We present the thermoelastic theory in Section II and describe the experimental investigation of the theory in Section III. The noise analysis and a theoretical prediction for the NEP are given in Section IV. In Section V, we comment on our findings from theoretical and experimental viewpoints. Finally, we consider the question of detector optimization in Section VI. Details of the calculations are given as appendices.

II. THEORY

The approach we will follow in presenting the thermoelastic theory
Figure 1 of PZT-PAS is shown in Fig. 1. The signal is generated when a beam of light is incident on an absorbing solid. The temperature of the illuminated volume increases, leading to the expansion of that region as
Figure 2 well as the outflow of heat (see Fig. 2a). The expansion of the central region causes displacement of the sample surface by two separate mechanisms. First, the enlargement of the central region causes the expan-

sion of both surfaces of the sample (see Fig. 2a). Second, in the case of strongly absorbing samples, the heat in the illuminated region decays spatially through the thickness of the sample (see Fig. 2b). Consequently, the front portion of the sample expands more than the rear, resulting in a bending of the sample. Such bending compresses the rear surface of the solid and opposes the general expansion shown in Fig. 2a. The bending also causes expansion of the front surface, thus adding to the expansion described in Fig. 2a. This displacement of the sample surface is then sensed by the transducer (see Fig. 3a) causing a voltage to develop in the z-direction between the two surfaces of the PZT.

Figure 3

A. Detector Geometry

Consider the geometry shown in Figs. 3a. and 3b. We treat two cases:

(1) Optically thick samples, where the light beam is not transmitted and the PZT is a slab covering the entire back surface of the solid (Fig. 3b),

(2) Optically thin samples, where the PZT is an annulus and is located on either side of the solid (Fig. 3a). As will be shown, the nature of the generating strain in the latter case is dependent upon the side on which the transducer is located.

B. Assumptions of the Theory

To simplify the problem, we assume the solid to be an isotropic, infinite, elastic layer. This approximation is reasonable since a focussed light beam typically is much smaller than the sample dimensions.

We also assume that the sample responds as if its boundaries were free from stress. This is a plausible assumption since the transducer is much thinner than the sample. In fact, for a transparent solid (Fig. 3a), the sample is free in its central region.

C. Temperature Distribution in the Sample

Assume we have a light source which is a square-wave intensity modulated laser beam with a Gaussian profile propagating along the z-axis (Fig. 4). Then the temperature distribution in the sample obeys the equation

Figure 4

$$\nabla^2 T - \frac{1}{\lambda} \frac{\partial T}{\partial t} = - \frac{Q(\vec{r},t)}{\kappa} \qquad (1)$$

with boundary conditions

$$\kappa \nabla T\big|_{z=0} = \kappa_1 T\big|_{z=0} \quad ; \quad \kappa \nabla T\big|_{z=\ell} = -\kappa_2 T\big|_{z=\ell} \qquad (2)$$

where T is the temperature, κ is the thermal conductivity, λ ($=\kappa/\rho C$) is the thermal diffusivity, ρC is the heat capacity/unit volume at constant volume, κ_1 and κ_2 are the surface conductivities of the front and back surfaces, respectively, and $Q(\vec{r},t)$ is the power/volume deposited by the laser beam.

Assuming that the light intensity decays exponentially in the sample, for the steady state temperature oscillating at the modulation frequency ω we have

$$Q(\vec{r},t) = \frac{2P}{\pi^2 a^2} \alpha e^{-r^2/a^2} e^{-\alpha z} \cos \omega t$$

$$= -\gamma \kappa \alpha e^{-r^2/a^2} e^{-\alpha z} \cos \omega t$$

where P is the incident power corrected for the sample reflectivity (R), a is the laser beam radius, α is the optical absorption length, ω is the angular modulation frequency, and $\gamma = -2P/\pi^2 a^2 \kappa$. The solution to Eqs. (1) and (2) is given by

$$T(z,r,t) = -\frac{P\alpha}{2\pi^2} e^{i\omega t} \int_0^\infty \frac{\delta d\delta e^{-\delta^2 a^2/4} J_o(\delta r)\left[-\alpha\cosh\xi(z-\ell) + \alpha e^{-\alpha\ell}\cosh\xi z + \xi e^{-\alpha z}\sinh\xi\ell\right]}{(-\delta^2+\alpha^2-K^2)(\sinh\xi\ell)(\kappa\xi)} + \text{c.c.} \tag{4}$$

where

$$K^2 = i\omega/\lambda$$

$$\xi = (\delta^2 + K^2)^{\frac{1}{2}}$$

and the conduction from the sample is negligible so we have set κ_1 and κ_2 equal to 0. A more detailed derivation is given in Appendix A.

D. Calculation of the Induced Strain

For an infinite free slab, the strain developed by a rise in temperature T should satisfy the equations

$$\nabla^2 u_r - r^{-2} u_r + e_{,r} - \frac{2(1+\nu)}{1-2\nu} a_t T_{,r} = 0$$

$$\nabla^2 u_z + \frac{1}{1-2\nu} e_{,r} - \frac{2(1+\nu)}{1-2\nu} a_t T_{,r} = 0 \tag{5}$$

where u_i is the displacement in the ith direction, ν is Poisson's ratio, a_t is the linear expansion coefficient of the solid,

$$e = u_{r,r} + r^{-1} u_r + u_{z,z}$$

and

$$\nabla^2 = \partial^2 r + r^{-1}\partial r + \partial^2 z \quad . \tag{6}$$

Setting the boundary conditions as $\sigma_{rz} = \sigma_{zz} = 0$ for $z = 0, \ell$ where σ_{ij} are the components of the stress tensor. Then the stress components given in terms of strain are

$$\sigma_{ii} = 2G\left(\varepsilon_{ii} + \frac{\nu}{1-2\nu}\, e - \frac{1+\nu}{1-2\nu}\, a_t T\right)$$
$$\sigma_{rz} = 2G\, \varepsilon_{rz} \tag{7}$$

where G is the shear modulus and ε_{ij} are the strain components, which are related to the displacement by

$$\varepsilon_{rr} = \frac{\partial u_r}{\partial r}, \qquad \varepsilon_{\theta\theta} = \frac{u_r}{r},$$
$$\varepsilon_{zz} = \frac{\partial u_z}{\partial z}, \qquad \varepsilon_{zr} = \frac{1}{2}\left(\frac{\partial u_r}{\partial z} + \frac{\partial u_z}{\partial r}\right). \tag{8}$$

To solve the stress equation, one defines a thermoelastic potential function Φ where $u_i = \partial_i \Phi$. Consequently, Eq. (7) and (8) reduce to

$$\nabla^2 \Phi = \frac{1+\nu}{1-\nu}\, a_t T .$$

For the boundary conditions stated above, it can be shown[22] that the stress solution is given by

$$\sigma_{ij}(r,z) = \int_{\text{slab}} T(\rho,z')\, \sigma^*_{ij}(\rho,z',r,z)\, d\rho\, dz' \tag{9}$$

where $T(\rho,z')$ is given in Appendix A and σ^*_{ij} is given in Appendix B.

E. PZT Strain Calculation

Now that we have solved for the stress induced by absorption of

light by the sample, we can determine the corresponding stress sensed by the PZT. For the piezoelectric material the governing equations are

$$\sigma_{ij} = C^{E}_{ijk\ell}\, u_{k\ell} - e_{kij}\, E_k$$

$$D_i = e_{ik\ell}\, u_{k\ell} + \varepsilon^{s}_{ik}\, E_k \tag{10}$$

where σ_{ij}, u_{ij}, E_k, D_i are the stress, the strain, the electric field, and the displacement; and $C^{E}_{ijk\ell}$, $e_{ik\ell}$, ε^{s}_{ik}, are the compliances, the piezoelectric constants, and the dielectric constants, respectively. The applicable boundary conditions in our case are σ_{zz}, σ_{xz}, $\sigma_{yz} \cong 0$, and $E_x = E_y = 0$.

Using these conditions, the symmetry of the transducer ceramic, Eq. (10), and the equation for $u_{z,z}$, we get[23]

$$D_3 = e^{P}_{31}\,(u_{r,r} + u_r/r) - \varepsilon^{P}_{33}\, E_3 \tag{11}$$

where

$$e^{P}_{31} = e_{31} - e_{33}\, C^{E}_{13} / C^{E}_{33}$$

$$\varepsilon^{P}_{33} = \varepsilon_{33} + e^{2}_{33} / C^{E}_{33}$$

Integrating (11) over the area, assuming that u_r is independent of z, and using the constant charge condition yields

$$\int D_3 dA = 0 = 2\pi e^{P}_{31} \int_0^{\infty} (u_{r,r} + u_r/r) r dr - \varepsilon^{P}_{33}\, \frac{VA}{L}$$

where V is the potential difference between electrodes and is independent of r. L(A) is the thickness(area) of the PZT. Finally, we get

$$V = \frac{2\pi e^{P}_{31} L}{\varepsilon^{P}_{33} A} \int_0^{\infty} (u_{r,r} + u_r/r)_{PZT}\, r\, dr$$

Noting that $u_{rr}=u_{r,r}$ and $u_{\theta\theta}=u_r/r$ for axial symmetry and that $u_{rr}+u_{\theta\theta}=u_{xx}+u_{yy}$ gives

$$V = \frac{2\pi\, e_{31}^P L}{\varepsilon_{33}^P A}\int_0^\infty (u_{xx}+u_{yy})_{PZT}\, r\, dr \quad . \tag{13}$$

Assuming that the displacements in the transducer are proportional to the displacements in the sample, then

$$V = \frac{2\pi\, e_{31}^P L}{\varepsilon_{33}^P A}\int_0^\infty (u_{xx}+u_{yy})_{\substack{\text{sample}\\ \text{at surface}}}\, r\, dr \quad . \tag{14}$$

From the following thermoelastic stress-strain relation

$$u_{ij} = a_t T\,\delta_{ij} + \frac{1}{2G}\left(\sigma_{ij} - \frac{\nu}{1+\nu}\, s\,\delta_{ij}\right) \tag{15}$$

where $S=\sigma_{xx}+\sigma_{yy}$, $\sigma_{zz}=0$,

we get

$$\langle u_{xx}+u_{yy}\rangle = 2a_t\langle T\rangle + \frac{1}{2G}\left(\langle S\rangle - \frac{2\nu\langle S\rangle}{1+\nu}\right)$$

$$= 2a_t\langle T\rangle + \frac{1-\nu}{E}\langle S\rangle$$

where $\langle\ \rangle$ denotes $2\pi\int_0^\infty r\,dr$.

From Appendix B we have

$$\langle S\rangle = \frac{Ea_t}{1-\nu}\left\{(1+\nu)\left[\langle T_o\rangle + (z-\ell/2)\langle\tau\rangle\right] - 2\langle T\rangle\right\} \quad . \tag{17}$$

This yields

$$V \simeq \frac{e_{31}^P L\, a_t}{\varepsilon_{33}^P A}(1+\nu)\left[\langle T_o\rangle + (z-\ell/2)\langle\tau\rangle\right]_{z=0,\ell} \quad . \tag{18}$$

This simple expression deserves further comment. The $\langle T_o\rangle$ term is the in-plate displacement due to the average temperature T_o. The second

term represents the sample buckling due to the average temperature gradient τ. When the transducer is on the laser side of the sample ($z=0$ in Fig. 4), the average term and the buckling term add since $\langle\tau\rangle < 0$. When the transducer is away from the laser ($z=\ell$) in Fig. 4, the terms subtract.

F. Implications of the Theory

Physically, the implications of Eq. (18) are more apparent if one considers various specific cases. In the following cases, $l_t = (2\lambda/\omega)^{\frac{1}{2}}$ is the thermal length, $l_o(=1/\alpha)$ is the optical length of the sample, and for simplicity, we have neglected surface conduction from the sample to the ambient air.

Case 1: For thermally and optically thick samples with the transducer located at $z=\ell$, we have with $\ell \gg l_t$ and $\ell \gg l_o$

$$V \simeq -\frac{2M\, Pa_t}{i\omega\ell(\rho C)_{sample}} \tag{19}$$

where

$$M = \frac{e_{31}^P L}{e_{33}^P A}\,\frac{2(1+\nu)}{\pi}$$

Case 2: For thermally thin but optically thick samples ($l_t \gg \ell \gg l_o$), we have

$$V \simeq \frac{M\, Pa_t}{i\omega\ell(\rho C)_{sample}} \tag{20}$$

again when the transducer is located at $z=\ell$.

Case 3: For thermally thick but optically thin samples ($l_o \gg \ell \gg l_t$), we have

$$V \cong \frac{M\, Pa_t}{i\omega\ell(\rho C)_{sample}} \left\{1 - e^{-\alpha\ell} \pm \frac{6}{\ell\alpha}\left[\left(1 - \frac{\ell\alpha}{2}\right) - e^{-\alpha\ell}\left(1 + \frac{\ell\alpha}{2}\right)\right]\right\} \tag{21}$$

where the negative sign applies for ($z=\ell$) the case when the transducer

is away from the laser beam and the positive sign is applicable when the transducer is towards the laser (z=0).

From the above cases we find the general form of the signal is

$$V \propto M a_t \frac{1}{\rho C} \frac{P}{\omega} ,$$

P/ω is the energy deposited per cycle, $1/\rho C$ converts the energy to a temperature, a_t transforms the temperature rise to a strain, and M is a voltage for a given strain.

Based on this theory, the following predictions are made.

1) The signal amplitude is proportional to the reflection corrected incident power.

2) The signal amplitude is related to the material parameters through the quantity $a_t(1-R)/(\rho C)_{sample}$. Note that the signal does not depend on Young's modulus or on the conductivity κ directly. The conductivity affects the signal as a result of its effect on the thermal length.

3) The signal amplitude has a $1/\ell$ dependence; hence thin samples tend to yield higher signals.

4) The signal has approximately $1/\omega$ dependence. The exact theory shows the frequency dependence closely approximates a $1/\omega^{0.9}$ dependence for thick metal samples.

5) The phase for metal data undergoes a 180^{o} phase shift as the thermal length becomes smaller than the sample thickness.

6) For small values of α, the photoacoustic signal is directly proportional to α. For high values α, the position of the PZT with respect to the direction of the incoming beam (z=0 or z=ℓ) yields significantly different results. When the transducer is away from the laser beam (z=ℓ), as α increases, the signal should decrease, eventually passing through zero and changing signs at higher values of α. On the other hand, when the transducer is attached to the sample surface towards the laser beam (z=0), it is predicted that the signal will show little saturation until α reaches very high values.

III. EXPERIMENTAL VERIFICATION OF THE THEORY

The predictions of our theory were tested experimentally for solids with a wide range of optical and thermal properties. The samples used were tungsten, tantalum, copper, glass coated with black paint, and didymium glass. The piezoelectric transducers (type 5502 lead zirconium titanate alloy) were obtained from Channel Industries and electrodes were attached to them with low temperature solder. For opaque samples (Fig. 3b), a 0.01 × 0.8 × 0.8cm PZT slab was used; for optically thin samples (Fig. 3a), PZT annuli were employed to minimize the scattering of the exciting light on the transducer itself. After testing several types of adhesive, we chose to employ Eastman 910[24] and a low viscosity epoxy[25] for the work reported below. Our experimental apparatus is shown in Fig. 5.

Figure 5

A. Verification of $1/\omega$ Dependence

Eq. (19) in Sec. II predicts that the amplitude of the photoacoustic signal is approximately inversely proportional to the modulation frequency of the

exciting light. By varying the chopping frequency using a computer, we found this to be the case for all of our samples over the modulation range tested (5-2000 Hz) as shown in Fig. 6.

Figure 6

B. Power Dependence of the Signal

The power dependence of the observed signal was verified by attenuating the intensity of the laser beam with calibrated filters. For various samples we found the signal to depend linearly on the power for over six orders of magnitude (Fig. 7). The minumum power we could detect was 0.1 μW for a signal to noise ratio of one. This is agreement with our predictions. By using a copper sample and continuously varying the wavelength of a dye laser, we verified the prediction that the signal is a linear function of the incident power when corrected for the reflectivity of the sample (Fig. 8).

Figure 7

Figure 8

C. Signal Dependence on the Optical Absorption Coefficient

The absorption bands of the didymium glass around the 5800 Å region were used to test the theoretical prediction of the signal dependence on the absorption coefficient (Sec. II). The sample absorption was measured simultaneously by transmission and by photoacoustics on two identical samples (Fig. 5). The experiments were performed for the transducer away and towards the laser beam. The agreement between the theory and the experimental results is good, as can be seen in Figs. 9,10. When the transducer is away from the beam ($z=\ell$), the relationship between the photoacoustic signal and optical absorption is highly nonlinear. The signal goes to zero at $\alpha\ell = 2$, where the compression due to the bending equals the expansion due to the heating. In Fig. 9 we show the abrupt

Figure 9

Figure 10

180^{o} phase shift by a negative amplitude. When the transducer is towards the laser beam (z=0) (Fig. 10), the bending and expansion terms add, increasing the observed signal. There is no saturation until high values of absorption.

D. The Dependence of Signal on Sample Thickness

To test the $1/\ell$ (Eq. 19) dependence, we varied the thickness by using varying lengths of black coated glass rods. We found that the signal exhibits approximately a $1/\ell$ dependence.

E. Signal Dependence on the Thermal Properties of the Sample

We have compared the relative magnitudes of the photoacoustic signal obtained from aluminum, tantulum, and copper samples of identical thickness (see Table I). Although the results are complicated by uncertainties concerning the reflectivity of the samples, the relative values are in agreement with the predictions. The experimental ratio of tungsten (which has a high E) to tantalum is smaller than predicted. However, the experimentally obtained tungsten signal is smaller than that obtained for tantalum, as is qualitatively predicted by our theory.

TABLE I

The phase of the metal samples shows the predicted 180^{o} phase shift at the predicted frequencies (Fig. 11). When the thermal diffusion length is on the order of the sample thickness, the phase shifts. Consequently, because Cu has a longer thermal diffusion length, the phase shifts at a higher frequency than tungsten.

Figure 11

We also point out that the absolute theoretical magnitudes of the

signal are within a factor of 2 of experimental values. Part of the discrepancy is due to greater absorption than was assumed in the theory. The greater absorption results from surface irregularities and contaminants. Finally, we verified that to within 5% the signal does not depend on the beam radius.

Having tested the theory on a variety of samples with a wide range of thermal and optical properties, we have found good agreement. Consequently, we believe that the theory is useful for quantitative calculations of the expected signal.

IV: NOISE ANALYSIS AND NOISE EQUIVALENT POWER

We next analyze the sources of noise and estimate a total noise equivalent power (NEP) for our detector. This discussion identifies factors which limit the sensitivity and serves as a guide for designing an optimized PAS-PZT detector. The noise factors we have considered are electronic noise, material dielectric loss noise, DC leakage noise, Brownian motion of the detector, and thermal noise. The first two are the most important, although DC leakage noise can become significant if the detector is improperly constructed.

A. Electronic Noise

Since the PZT is a high impedance device, the preamp should contain an FET front end. Consequently, we follow the approach of Van der Ziel[26] and Byer[27] for constructing a noise equivalent circuit including an FET (see Fig. 12). Figure 12 One can neglect R_{dc}, R_{ac} (providing no low resistance path shunts the transducer), and C_a as far as their effect on the impedance of the network. Furthermore, since one is typically operating

at a frequency such that $1/\omega C << R_{inp}$, the total impedance of the network is $Z = 1/i\omega C$. The rms noise voltage due to the amplifier is given by:

1) $V_I = i_n |Z| \Delta f^{\frac{1}{2}}$ from the current noise

2) $V_V = e_n \Delta f^{\frac{1}{2}}$ from the voltage noise

where

$i_n^2 = 2eI_g$

$e_n^2 = (8k_BT/3g_m)(1 + f_o/f) + (4k_BT)/R_L\, g_m^2$

I_g - gate leakage noise

g_m - FET transconductance

f_o - 1/f noise corner frequency

R_L - load resistor

T - amplifier temperature

Δf - lock-in bandwidth.

Since the signal for all cases has the form

$$V = J\, P\, |Z| / \ell$$

where

$$J = e_{31}^P\, a_t (1+\nu)/(C\rho)_{sample} ; \quad Z = 1/\omega C = L/\omega \varepsilon_{33}^P A$$

we get the contributions to the NEP,

$$(NEP)_I = i_n\, \ell/J \tag{22}$$

$$(NEP)_V = e_n\, \ell\, \varepsilon_{33}^P A/JL \tag{23}$$

At low frequencies since $e_n \sim 1/\omega^{\frac{1}{2}}$. Then $(NEP)_V \propto \omega^{\frac{1}{2}}$.

B. PZT Material Noise Sources

The dielectric loss and leakage noise contributions are

$$(NEP)_D = \ell/J \left(\frac{4k_BT\, \omega\, \varepsilon_{33}^P A\, \tan\delta}{L} \right)^{\frac{1}{2}} \tag{24}$$

and

$$(NEP)_{DC} = \ell/J \left(\frac{4k_BT\, \sigma\, A}{L} \right)^{\frac{1}{2}} \tag{25}$$

where $\tan\delta$ is the dielectric loss tangent and σ is the volume resistivity.

C. Fundamental Noise Sources

The NEP due to fluctuations of the temperature of the transducer is

$$(NEP)_{thermal} = \frac{(4k_B\, g_H)^{\frac{1}{2}}\, T\mathcal{P}\ell}{(\rho C)_{PZT}\, LJ} \tag{26}$$

and the NEP due to Brownian motion is approximately

$$(NEP)_{Brownian} = \left(\frac{4k_B\, TA\ell\omega\, e_{31}^{P}}{L^3 Q \rho_{PZT}\, \omega_o^3 J}\right)^{\frac{1}{2}} \tag{27}$$

where g_H is the thermal conductance with the surroundings, $\mathcal{P}$ is the pyroelectric coefficient for the transducer, Q is the Q of the transducer, and ω_o is the first resonance of the PZT.

D. Numerical Results

We consider a numerical example. For our PZT, $C=1.2\times10^{-8}$F, $A=1\times10^{-5}\,m^2$, $\tan\delta = 0.01$, $L=1.78\times10^{-4}$ m, $\sigma = 10^{-11}\,\Omega^{-1}cm^{-1}$, $g_H=7.019\times10^{2}$ J/sec/°C, $\mathcal{P}=0.1\times10$ coul/cm^2/°C, $\rho=5.2$ g/cm^3, $C_v=.4$ J/g/°C, $Q=75$, $\omega_o=2\pi(5\times10^5)$. Using the noise figures for our lock-in amplifier we get the noise shown in Table II. The measured system noise was 17 nV/Hz$^{\frac{1}{2}}$ at 16.6Hz for a totally isolated detector. The agreement between the theoretical and measured noise is fortuituous since many factors such as $\tan\delta$ are estimates. However, these values are useful for assessing the relative contributions of the different noise sources.

TABLE II

The measured voltage responsivity was giving an $NEP_V=5\times10^{-8}$ W at 16.6 Hz. If the dielectric loss tangent does not become significantly

large at lower frequencies, operation at 5 Hz can improve this figure somewhat. In our experiments, we achieved an NEP of 1×10^{-7}W for thin metals and 6×10^{-7}W for transparent samples.

V. DISCUSSION

Despite the complex nature of the problem, we have shown that our three-dimensional treatment yields a simple expression (Eq. 18) which quantitatively describes the experimentally observed PZT photoacoustic signal.

We show that the PZT measures the temperature distribution within the sample. There is no complication due to the delay or propagation of a thermally induced sound wave. For thermally non-conductive samples, the temperature distribution is proportional to the heat deposited per volume.

It is important to point out that our theory is not a linearized theory and it does not assume that the sample is thin, although in thin sample cases one can derive an identical expression using thin plate theory[28]. Our theory is applicable for $\alpha\ell$ as high as 10 for thermally non-conductive media.

The applicability of this theory may be readily extended beyond the limitations of our assumptions and without appreciably altering our findings. First, the assumption of an infinite transducer can be eliminated by numerically integrating Eqn. (B7) over r from the inner radius to the outer radius of the annular PZT. Second, it can be shown that the theory is approximately correct for finite samples as well. If the transducer covers the entire sample surface, we find that the same

solution presented above is valid when the following substitutions are made:

$$\int_0^\infty \delta d\,\delta \longrightarrow \sum_{n=1}^{\infty} \frac{2}{d^2} J_o(y_{0n}) \quad ; \quad \text{and} \quad \delta \rightarrow y_{0n}/d \quad ,$$

where y_{0n} satisfy $J_o(y_{0n})=0$, $n=1,\infty$ and d is the radius of the sample. The solution obtained by such a substitution is approximate in that $\sigma_{rr}=0$ at the boundary while σ_{rz} is not. Finally, one may take the heat diffusion through the thin layer of adhesive into account by solving the heat flow equations in all regions. The resulting temperature distribution may be substituted into Eqn. (18).

Several simplifications of the theory which cannot easily be eliminated should be noted. The first one involves neglecting the interaction between the sample and the PZT. If the sample is thick compared to the PZT and the PZT is relatively compliant, the transducer measures the strain of the sample as assumed by the theory. If, however, the transducer thickness is comparable to or larger than that of the sample, the theory may be expected to break down for three reasons. First, the transducer will measure the stress of expression Eqn. (B8) in the sample rather than the strain. Second, the expansion of the sample will be altered. Finally, the neutral surface (the surface of zero displacement) for the transducer-sample combination is located within the transducer. This causes a reduction in the signal since the piezoelectric material on one side of the neutral surface expands while it compresses on the other sides. These two contributions tend to cancel out, reducing the net signal. Consequently, although the signal to noise ratio improves as the transducer gets thicker, the theory may no longer be

valid.

A second limitation concerns the contribution of the pyroelectric effect. If significant amounts of heat are transmitted to the transducer, the transducer would develop thermal stresses of its own and produces a voltage due to the pyroelectric effect. This would become significant only in the case of very low chopping frequencies, high thermal conductivities of the sample, and thermally conductive adhesive.

Finally, the transducer restricts large bending motions even if it is relatively compliant or thin compared to the sample. Hence, one expects that at high absorptions and low diffusivities the bending contribution may be somewhat less than that theoretically predicted.

From an experimental viewpoint, the main factor limiting the detector performance is the background signal which results from the scattering of light on the PZT. This background signal is wavelength dependent and can be minimized, for example, by depositing a layer of highly reflecting material on the PZT before coupling it to the sample.

VI CONSIDERATIONS FOR DETECTOR OPTIMIZATION AND FINAL REMARKS

Eqs. (22)-(27) do not yield an absolute value for the NEP. However, they do give the relative dependence of the NEP on various important parameters and can be used for the purpose of optimizing the PZT-PAS detector. In Table III, we give a set of rules of thumb for an optimized detector.

TABLE III

In conclusion, we have presented and experimentally verified a theoretical model which quantitatively accounts for the PZT photoacous-

tic signal. This should enhance the utility of PZT-PAS as a useful spectroscopic tool. We have also shown that the PZT directly detects heat-induced strain caused by the absorption of electromagnetic radiation.

ACKNOWLEDGMENTS

We thank H. Birecki, R. M. White, and C. Germano for stimulating discussions, R. Gerlach for his help in the experimental work, and Z. Yasa, D. Wake, and M. Jackson for their assistance and support. This work was done under the auspices of the U. S. Department of Energy.

APPENDIX A: SOLUTION FOR THE TEMPERATURE

The equations to be solved are

$$\nabla^2 T - \frac{1}{\lambda}\frac{\partial T}{\partial t} = -Q(r,t)/\kappa \qquad \text{(A1)}$$

with the boundary conditions

$$\kappa \left.\frac{\partial T}{\partial z}\right|_{z=0} = \kappa_1 T|_{z=0} \quad , \qquad \kappa \left.\frac{\partial T}{\partial t}\right|_{z=\ell} = -\kappa_2 T|_{z=\ell} \qquad \text{(A2)}$$

where κ_1 and κ_2 are the surface conductivity for the front and the back medium respectively. If we let $T = \frac{1}{2} T e^{i\omega t} + \text{c.c.}$, we find that

$$\nabla^2 \tilde{T} - K^2 \tilde{T} = \gamma\, e^{-r^2/a^2}\, e^{-\alpha z} \qquad \text{(A3)}$$

with

$$i\omega/\lambda = K^2$$

and

$$\gamma = -2P\alpha/\pi^2 \kappa a^2$$

To solve (A3), we find a particular solution $\tilde{T}_p$ and a homogeneous

solution $\tilde{T}_{hom}$. Letting

$$\tilde{T}_p = \int_0^\infty \delta C(\delta) e^{-\alpha z} J_o(\delta r)\, d\delta \tag{A4}$$

and substituting (A4) into (A3) gives

$$\tilde{T}_p = \int_0^\infty \frac{\gamma R(\delta)\, e^{-\alpha z}\, J_o(\delta r)\, \delta\, d\delta}{\alpha^2 - \delta^2 - K^2} \tag{A5}$$

where

$$R(\delta) = \frac{a^2}{2}\, e^{-\delta^2 a^2/4} \quad . \tag{A6}$$

For the homogeneous equation we let

$$\tilde{T}_{hom} = \int_0^\infty \delta J_o(\delta r)\left\{ A(\delta) e^{\xi z} + B(\delta) e^{-\xi z} \right\} d\delta \tag{A7}$$

with

$$\xi = (\delta^2 + K^2)^{1/2} \quad . \tag{A8}$$

We find $A(\delta)$ and $B(\delta)$ by requiring

$$\tilde{T} = \tilde{T}_{hom} + \tilde{T}_p \tag{A9}$$

to satisfy the boundary conditions (A2). Solving for $A(\delta)$ and $B(\delta)$ and substituting into (A9) gives

$$\begin{aligned} \tilde{T}(r) = -\int_0^\infty \frac{\gamma R(\delta)\delta\, J_o(\delta r)\, d\delta}{[-\delta^2 + \alpha^2 - K^2]D} \Big\{ & (b-1)(g+r)\, e^{-\xi(\ell - z)} \\ & - (b+1)(g+r)\, e^{\xi(\ell - z)} + (1+g)(r-b)\, e^{-\alpha\ell + \xi z} \\ & + (1-g)(r-b)\, e^{-\alpha\ell - \xi z} - (1-g)(1-b)\, e^{-\xi\ell - \alpha z} \\ & + (1+g)(1+b)\, e^{\xi\ell - \alpha z} \Big\} \end{aligned} \tag{A10}$$

where

$$b = \kappa_2/\kappa\xi = [K_2(\rho C)_2\omega]^{1/2}/\kappa\xi \quad ; \quad g = \kappa_1/\kappa\xi = [\kappa_1(\rho C)_1\omega]^{1/2}/\kappa\xi \quad ;$$

$$r = \alpha/\xi \quad ; \quad \text{and} \quad D = (1+g)(1+b)e^{\xi\ell} - (g-1)(b-1)\, e^{-\xi\ell}$$

and $\kappa_i, (\rho C)_i$ are the conductivities and heat capacity/volume for the ith medium. We note in passing that letting z=0 gives the same results as the one-dimensional theory by Rosencwaig and Gersho[10]. However, our approach is simpler since we have to solve the heat equation in one region with one boundary condition at each interface.

APPENDIX B: GREEN'S FUNCTION SOLUTION TO THE STRESS PROBLEM

We approximate our sample by an infinite layer with stress free boundaries. A Green's function for an annular temperature distribution in a solid (see Fig. 13) is given in Ref. 22. In the following (*) denotes a Green's function, ($\bar{\sigma}$) denotes an inhomogeneous solution, and ($\bar{\bar{\sigma}}$) denotes a homogeneous solution. The sum of the stress distribution in the solid is given by

Figure 13

$$\sigma(r,z';t) = \sum_{j,i=1}^{2} \delta_{ij}(r,z';t) = 2\pi \int_0^\infty \rho d\rho \int_{-\ell/2}^{\ell/2} d\varepsilon \; T(\rho,\varepsilon;t)\sigma^*(r,z';\rho,\varepsilon) \tag{B1}$$

where the Green's function has the form

$$\sigma^*(r,z';\rho,\varepsilon) = \bar{\bar{\sigma}}^*_{rr}(r,z';\rho,\varepsilon) + \bar{\bar{\sigma}}^*_{\theta\theta}(r,z';\rho,\varepsilon) + \bar{\sigma}^*_{rr}(r,z';\rho,\varepsilon) + \bar{\sigma}^*_{\theta\theta}(r,z';\rho,\varepsilon) \tag{B2}$$

$$\bar{\bar{\sigma}}^*_{rr} + \bar{\bar{\sigma}}^*_{\theta\theta} = \int_0^\infty \delta^2 \rho \; J_o(\delta r) \; J_o(\delta\rho) \; F(\varepsilon,z',\delta) \; d\delta \tag{B3}$$

where

$$F(\varepsilon,z',\delta) = \frac{2G}{1-2\nu}\left\{2\nu \sinh \delta z' + \delta z' \cosh \delta z' + \left(2 - \frac{\delta\ell}{2}\coth\frac{\delta\ell}{2}\right)\sinh \delta z'\right\}$$
$$\times \left\{(1-2\nu)\frac{\sinh \delta\varepsilon \; m \sinh \delta\ell/2}{\sinh \delta\ell/2 \; (\sinh \delta\ell - \delta\ell)}\right\}$$
$$+ \frac{2G}{1-2\nu}\left\{2\nu \cosh \delta z' + (2-\delta\ell/2 \tanh \delta\ell/2)\cosh \delta z' + \delta z' \sinh \delta z'\right\}$$
$$\times \left\{(1-2\nu)\frac{\cosh \delta\varepsilon \; m \sinh \delta\ell/2}{\cosh \delta\ell/2(\delta\ell + \sinh \delta\ell)}\right\} . \tag{B4}$$

and

$$\bar{\sigma}^{*}_{rr} + \bar{\sigma}^{*}_{\theta\theta} = -2G \left\{ m\delta(r-\rho)\,\delta(z-\varepsilon) + \frac{2m\rho}{\ell} \sum_{n=1}^{\infty} a_n^2 \times \begin{bmatrix} \sin a_n\varepsilon \sin a_n z & (n \text{ even}) \\ \cos a_n\varepsilon \cos a_n z & (n \text{ odd}) \end{bmatrix} \int_0^{\infty} \frac{\delta J_o(\delta\rho)\; J_o(\delta r)}{a_n^2 + \delta^2}\, d\delta \right\} \qquad (B5)$$

with $a_n = n\pi/\ell$ and $m = \frac{1+\nu}{1-\nu} a_t$.

We can write (A10) as

$$\tilde{T}(\rho,\varepsilon,\omega) = \int_0^{\infty} \delta' J_o(\delta'\rho)\; G(\varepsilon,\delta')\; d\delta' \qquad . \qquad (B6)$$

We require the quantity

$$\langle S \rangle = 2\pi \int_0^{\infty} \sigma(r,z';t)\; r dr \quad .$$

Substituting (B3), (B5), (B6) into (B1) and using the orthogonality of the Bessel functions we get the following

$$\langle S \rangle = \int_{-\ell/2}^{\ell/2} d\varepsilon \int_{PZT} r dr \int_0^{\infty} \delta' d\delta'\; G(\varepsilon,\delta')\delta' J_o(\delta' r)\; F(\varepsilon,z',\delta') + \int_0^{\infty} r dr \int_{-\ell/2}^{\ell/2} d\varepsilon \int_0^{\infty} \rho d\rho (\bar{\sigma}^{*}_{rr} + \bar{\sigma}^{*}_{\theta\theta})\; T(\varepsilon,\rho) \qquad . \qquad (B7)$$

At this point, one can either numerically integrate the above expression or one can assume that the transducer covers the entire surface of the sample. This allows two more integrals to be performed giving

$$\langle S \rangle = 2\pi \int_0^{\infty} r(\sigma_{rr} + \sigma_{\theta\theta}) dr = \frac{Ea_t}{1-\nu} \left\{ \langle (1+\nu)[T_o + (z - \ell/2)\tau] - 2T \rangle \right\} \qquad (B8)$$

where $\langle f(r) \rangle$ denotes $2\pi \int_0^{\infty} r\, f(r) dr$.

REFERENCES

1. L.B. Kreuzer, J. of Appl. Phys., 42, 2934 (1971).

2. J.G. Parker and Ritke, J. Chem. Phys., 59, 3713 (1973).

3. R.D. Kamm, J. Appl. Phys. 47, 3550 (1976).

4. R. Gerlach and N.M. Amer, Appl. Phys. Lett., 32, 228 (1978).

5. L.J. Thomas, M. Kelly, and N.M. Amer, Appl. Phys. Letters, 32, 736 (1978).

6. D. Wake and N.M. Amer, Appl. Phys. Lett., 34, 379 (1979).

7. J.F. McClelland and R.N. Kniseley, Appl. Phys. Lett., 28, 467 (1976).

8. G.C. Wetsel, Jr. and F.A. McDonald, J. Acoust. Soc. Am. 60, S52 (1976).

9. C.K.N. Patel and A.C. Tam, Appl. Phys. Lett., 34,760 (1979).

10. A. Rosencwaig and A. Gersho, J. Appl. Phys. 47, 64 (1976).

11. L.C. Amodt, J.C. Murphy, and J.G. Parker, J. Appl. Phys., 48, 927 (1977).

12. H.S. Bennett and R.A. Forman, Appl. Optics 15, 1313 (1976).

13. H.S. Bennett and R.A. Forman, J. Appl. Phys. 48, 1432 (1977).

14. J.G. Parker, Appl. Optics, 12, 2974 (1973).

15. S.A. Schleusener, J.D. Lindberg, K.O. White, and R.L. Johnson, Appl. Opt., 15 2546 (1976).

16. Z. Yasa, N.M. Amer, H. Rosen, A.D. Hanson, and T. Novakov, Appl. Optics, 18, 2528 (1979).

17. R.M. White, Jour. of Appl. Phys., 34, 3559(1963).

18. J.B. Callis, J. Res. Natl. Bur. Stand. A 80, 413 (1976).

19. A. Hordvik and H. Schlossberg, Appl. Opt. 16, 101 (1977).

20. M.M. Farrow, R.K. Burnham, M. Auzannean, S.L. Olsen, N. Purdie, and E.M. Eyring, Appl. Optics 17, 1093 (1978).

21. G.C. Wetsel, Jr. Presented at Topical Meeting on Photacoustic Spectroscopy, Iowa State University, Ames Iowa, 1979 (unpublished).

22. W. Novacki, Thermoelasticity, (Pergamen Press Ltd., Oxford, 1962).

23. A.H. Meitzler, H.M. O'Bryan, Jr., and Harry F. Tiersten, IEEE Trans. on Sonics and Ultrasonics, SU-20, 233 (1973).

24. Eastman 910 is a cynoacrylate adhesive manufactured by Eastman Company.

25. TRA-CON 2113 low viscosity epoxy manufactured by TRA-CON.

26. A. Van der Ziel, Noise in Measurements, (John Wiley and Sons, New York, 1976).

27. C.B. Roundy and R.I. Byer, J. Appl. Phys., 44, 929 (1973).

28. The same result is obtained if one uses thin plate theory. One solves for the longitudinal expansion of the plate and the buckling of the plate assuming that they are uncoupled. The solution, unlike the one presented above is valid throughout the sample thickness. For further details of thin plate theory see Z. Zudans, T.C. Yen, and W.H. Stiegelman, Thermal Stress Techniques, (Elsevier, 1956).

Table I. Results for various metals.

Metal	Theory(mV)	Experiment(mV)
Cu	1.58	3.1
Ta	3.71	7.25
Al	5.94	11.2
W	2.0	3.0
Ratio	**Theory**	**Experiment**
Cu/Ta	.426	.46
Ta/Al	.62	.65
Al/W	2.98	3.73

Table II. Noise contributions ($nV/\sqrt{Hz}$).

Source	Magnitude $(nV/Hz)^{\frac{1}{2}}$
Electronic	12.9
Dielectric loss	11.42
DC leakage	0.61
Brownian motion	1.37
Thermal	1.67
Total rms	17.4

Table III. Recomendations for signal to noise optimization.

Category	Quantity	Recommendation
Electronic	g_m	large
	1/f noise	small
	I_g	small
	PZT Area	small
	PZT Thickness	large[a]
	Sample Thickness	large[a]
PZT Properties	e_{31}^P	large
	$\tan\delta$	small
	ε_{33}^P	small
	σ	small
	φ	small
Sample Properties	a_t	large
	$(\rho C)_{sample}$	small
	T_{PZT}	low
Modulation Frequency	ω	low[b]

[a]The sample should not be much thinner than the PZT, otherwise the neutral surface of the PZT-sample configuration will occur within the PZT leading to a reduction of the signal.

[b]The amplifier voltage NEP goes down as the frequency until the amplifier current noise NEP dominates. Further reduction will not improve the signal to noise ratio because of the difficulty in isolating low frequency vibrations.

FIGURE CAPTIONS

Fig. 1. Flowchart showing steps in the calculation. The symbols are defined in the text and in the appendices.

Fig. 2. Sources of surface strain. Transducer may be attached to either side of the sample.

Fig. 3. Transducer-sample geometry. 3a) Configuration used for transparent samples. 3b) Configuration for opaque samples.

Fig. 4. Temperature distribution in sample with boundary conditions.

Fig. 5. Experimental apparatus. The two samples are identical.

Fig. 6. PAS signal vs. modulation frequency. Both full theory (no thermal or optical length approximations are made) and experiment show slightly less than a $1/\omega$ dependence ($1/\omega^{+0.9}$).

Fig. 7. PAS signal vs. incident laser power.

Fig. 8. Normalized PAS signal of Cu vs. wavelength. Spectra is normalized to the 0.6μ value.

Fig. 9. PAS signal vs. $\alpha\ell$. Inset shows direction of incident light in relation to the transducer. At $\alpha\ell \sim 2$, the phase undergoes a 180^{o} phase shift which is indicated by making the signal amplitude negative.

Fig. 10. PAS signal vs. $\alpha\ell$. The sample is the same as that in Fig. 9.

Fig. 11. PAS Phase vs. modulation frequency.

Fig. 12. Equivalent circuit of detector for signal and noise. Q-charge generated by strain. $I_1=(4k_BT\Delta f/R_{dc})^{\frac{1}{2}}$ - current noise due to R_{dc}, C-transducer capacitance, $R_{ac}=\tan\delta/\omega C$ - AC loss resistance, $I_2=(4k_BT\omega C \tan\delta)$-current noise due to R_{ac}, $1/C_a$-amp input capacitance, R_{inp}-amp input impedance, $I_3=i_n\Delta f^{\frac{1}{2}}$-amplifier noise current, $V=e_n\ \Delta f^{\frac{1}{2}}$- amplifier noise voltage, R_L-load resistor.

Fig. 13. Geometry for stress calculation. 1(2) is the front(back) medium and r is measured from the beam center.

CALCULATION FLOW CHART

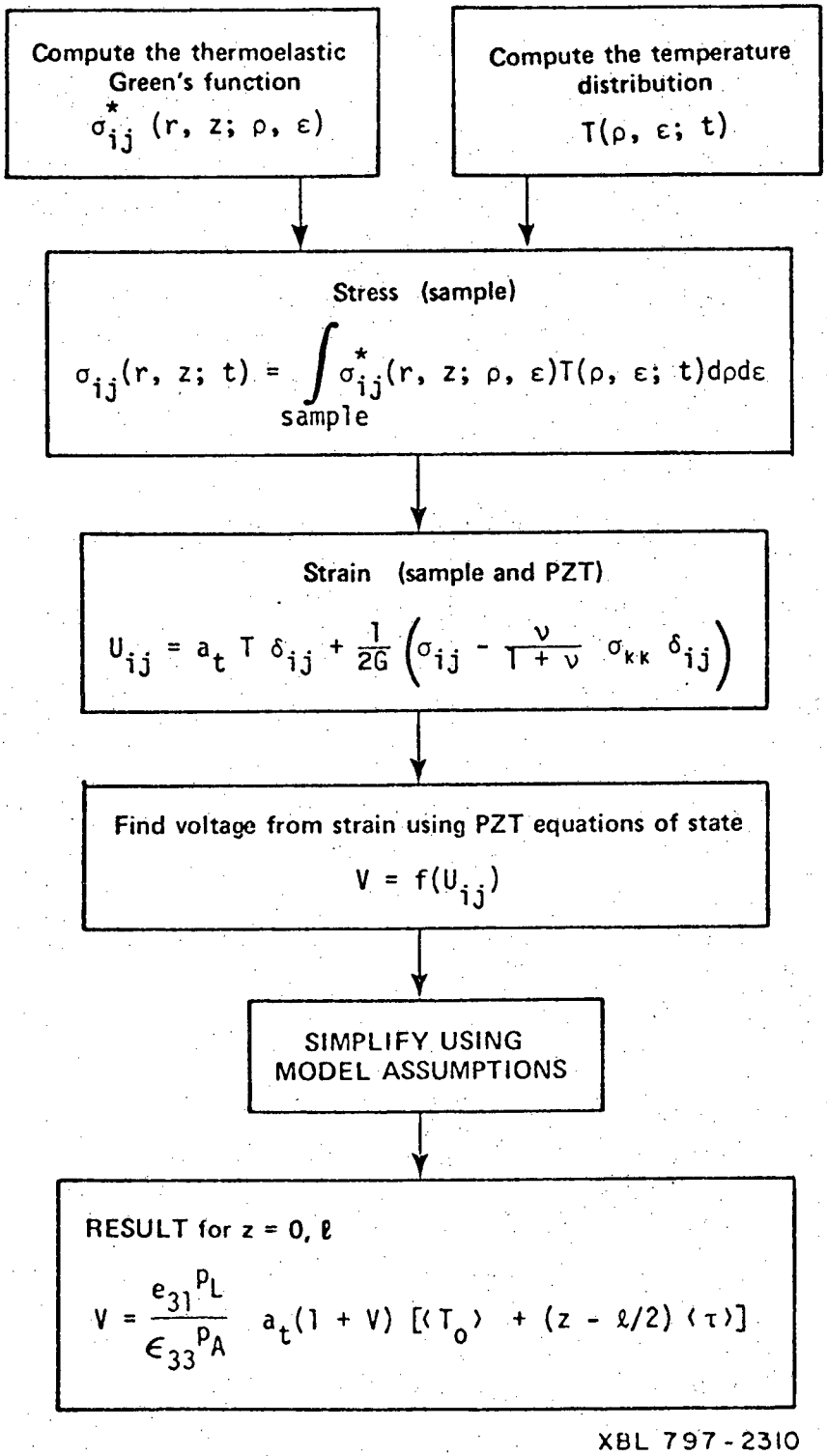

(Fig. 1)

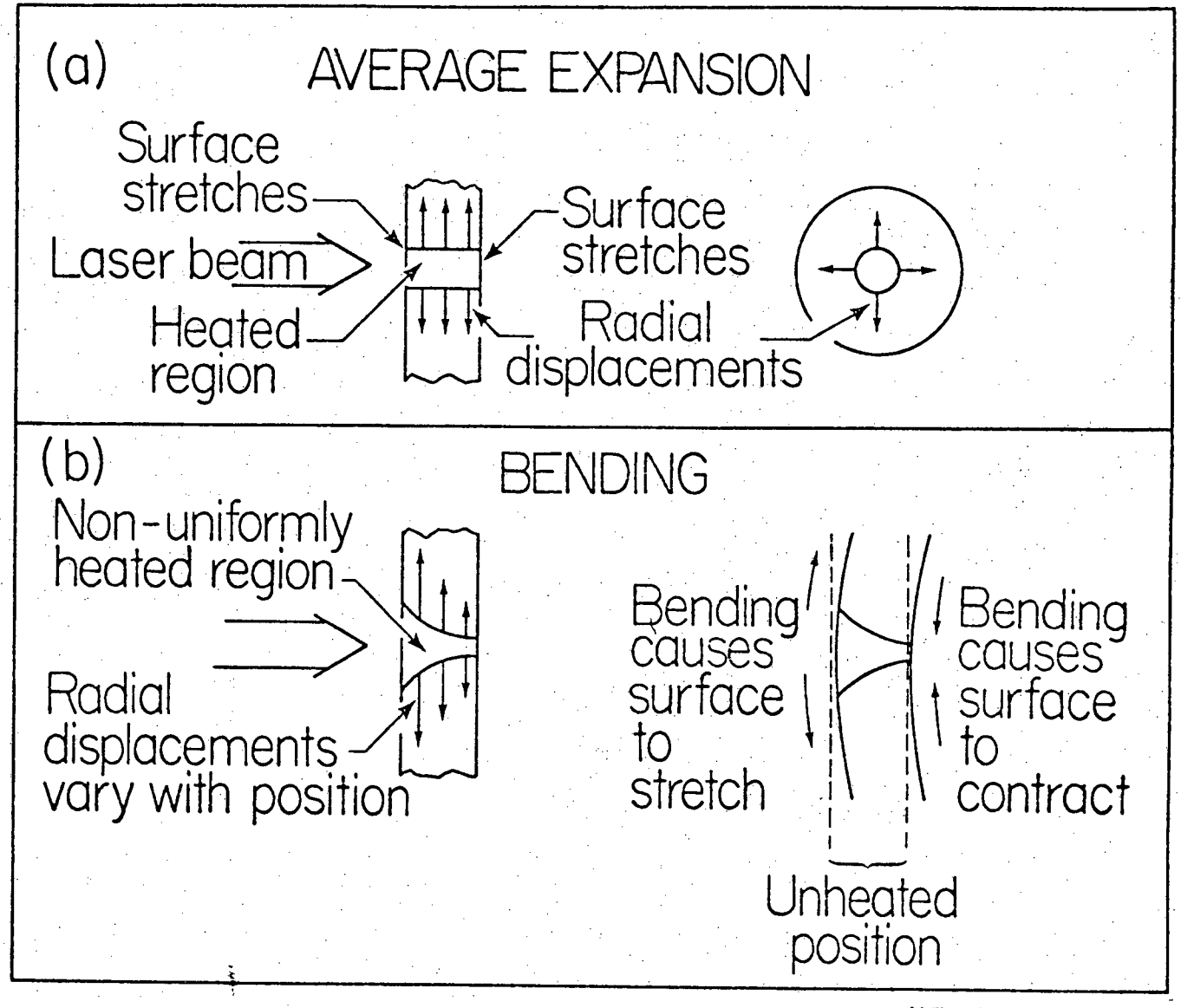

XBL 797-2315

(Fig. 2)

PZT-Sample Geometry

(a.) Transparent Samples

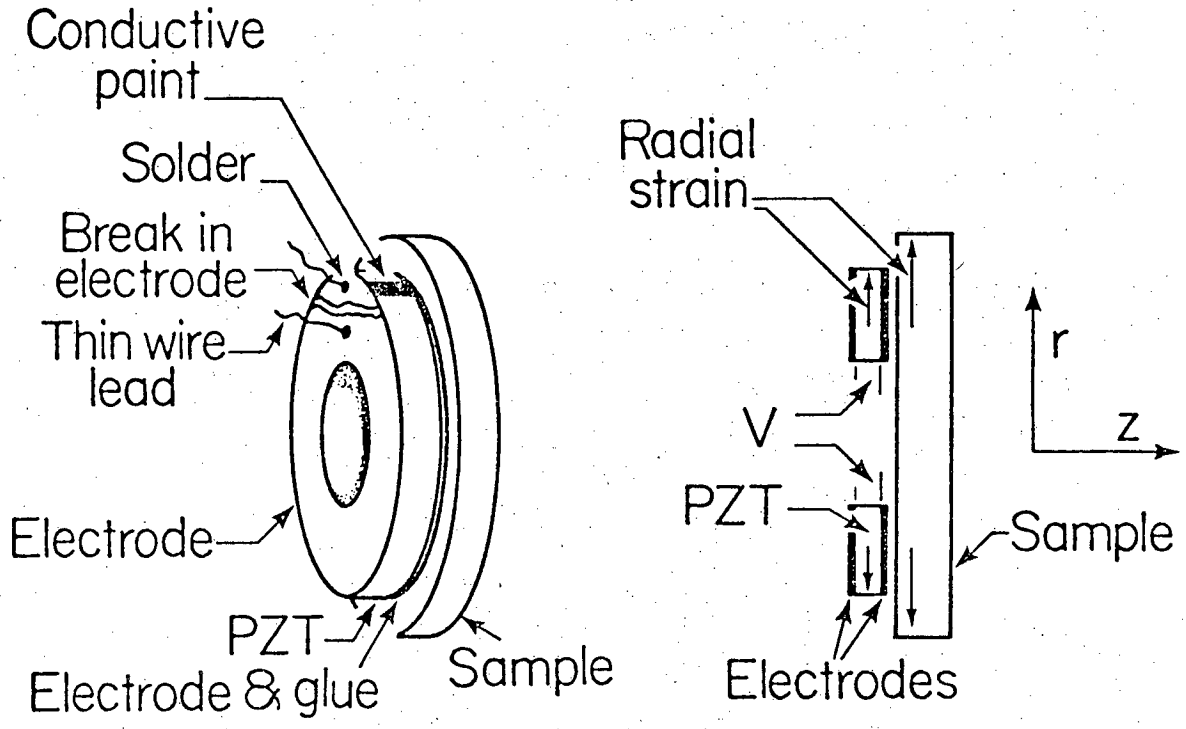

(b.) Opaque Samples

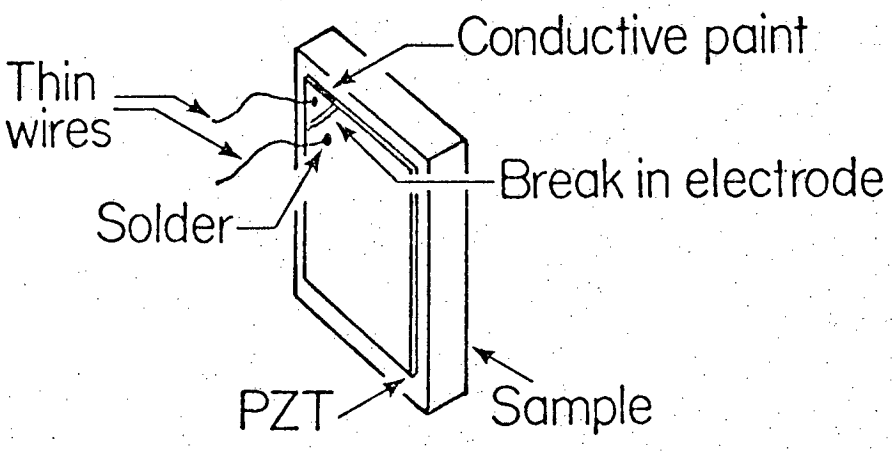

XBL797-2316

(Fig. 3)

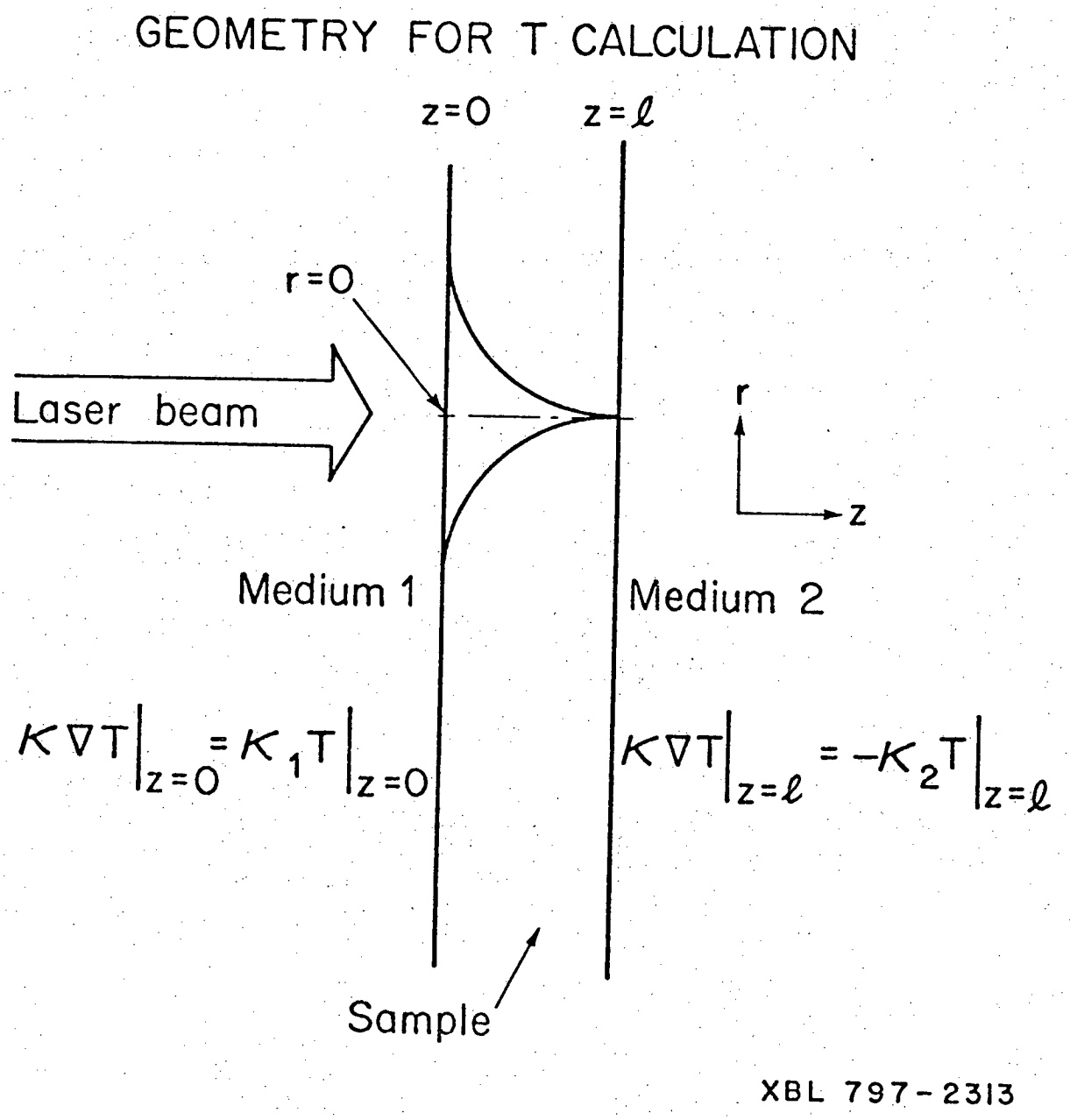
GEOMETRY FOR T CALCULATION
z=0
z=ℓ
r=0
Laser beam
r
z
Medium 1
Medium 2
$K\nabla T\big|_{z=0} = K_1 T\big|_{z=0}$
$K\nabla T\big|_{z=\ell} = -K_2 T\big|_{z=\ell}$
Sample
XBL 797-2313

(Fig. 4)

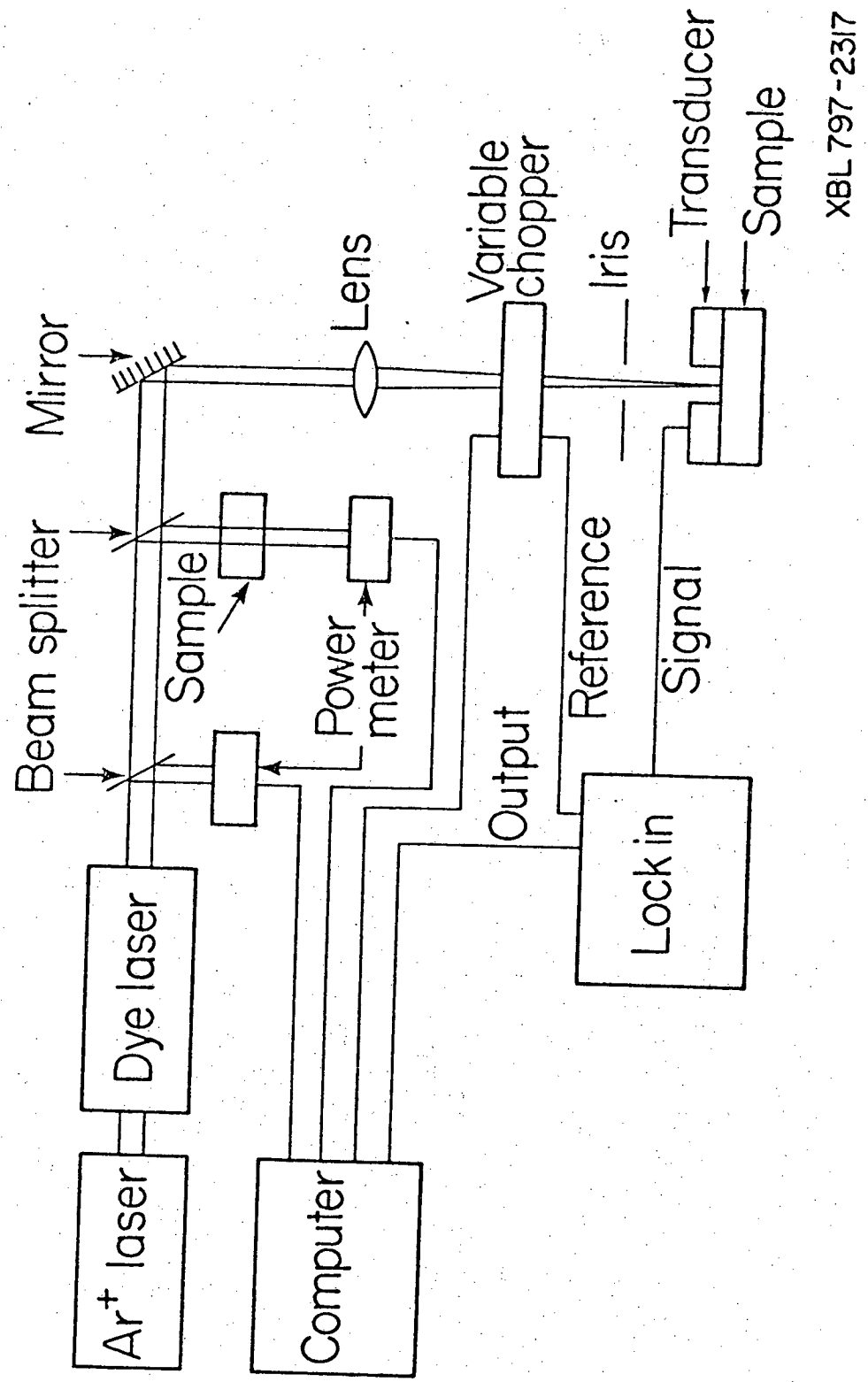
Mirror
Lens
Variable chopper
Iris
Transducer
Sample
XBL 797-2317
Beam splitter
Sample
Power meter
Reference
Signal
Output
Lock in
Dye laser
Ar+ laser
Computer

(Fig. 5)

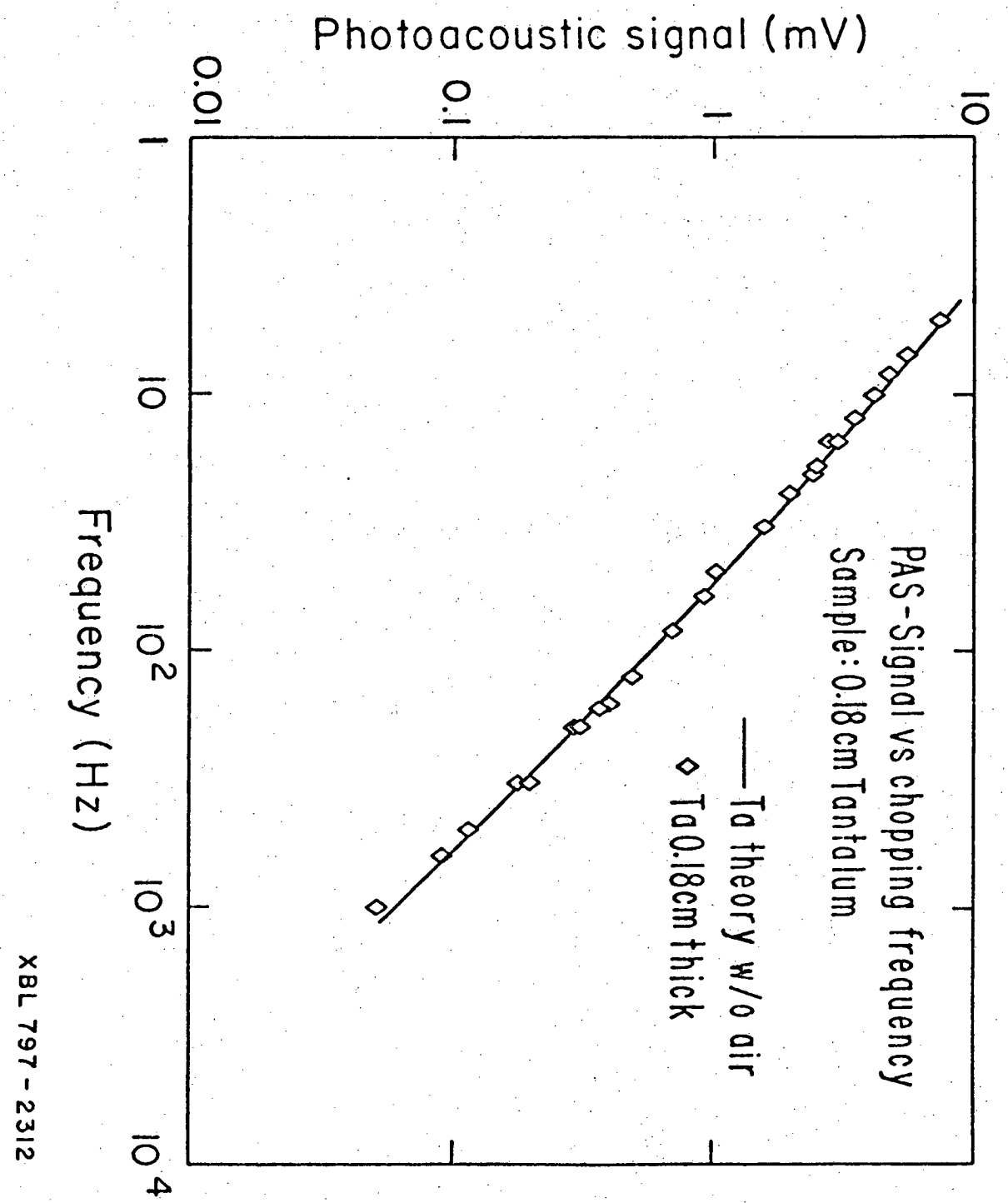
Photoacoustic signal (mV)
0.01
0.1
1
10
Frequency (Hz)
1
10
10^2
10^3
10^4
PAS-Signal vs chopping frequency
Sample: 0.18 cm Tantalum
— Ta theory w/o air
◇ Ta 0.18 cm thick
XBL 797-2312

(Fig. 6)

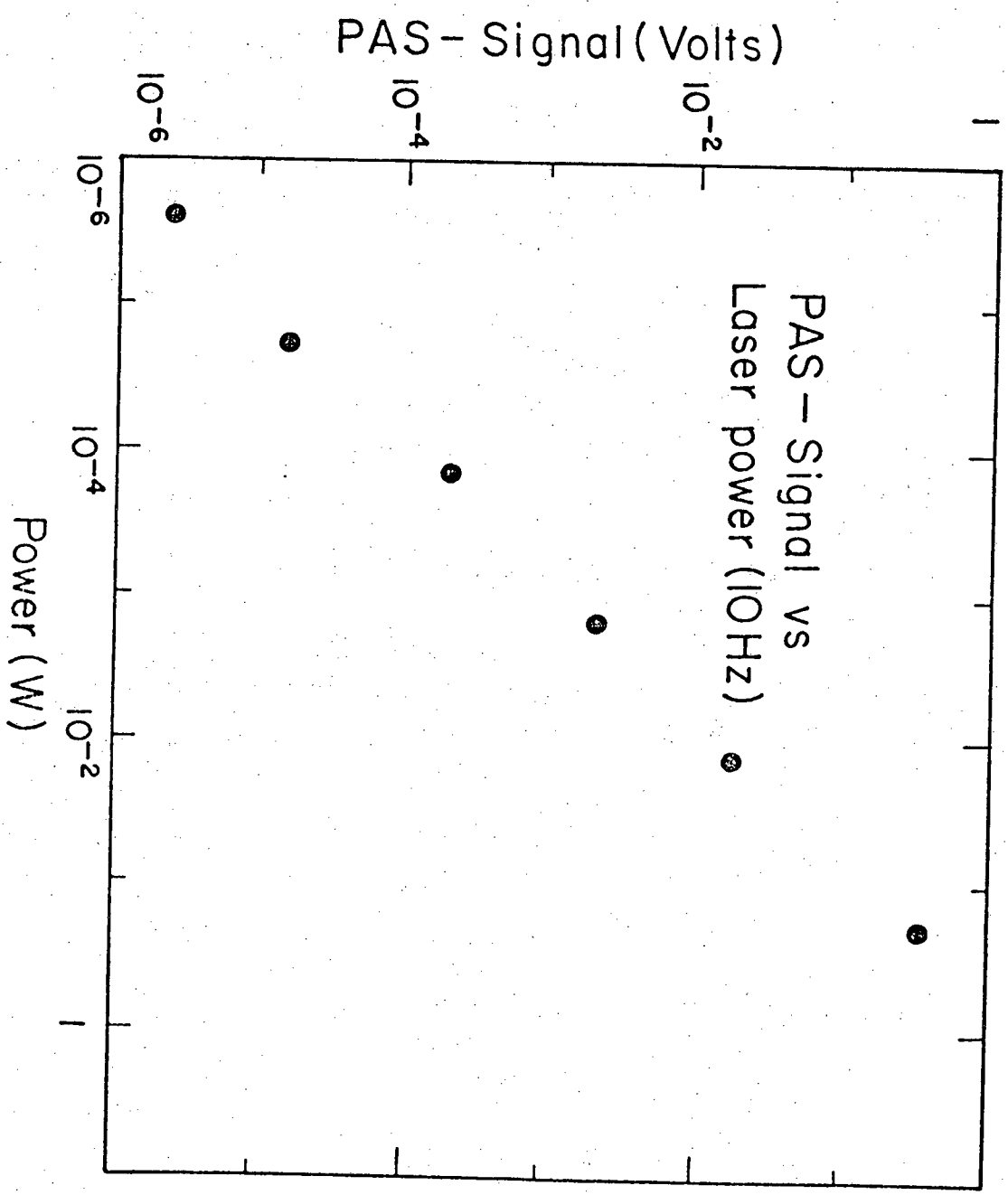
PAS - Signal (Volts)
10⁻⁶
10⁻⁴
10⁻²
1
PAS - Signal vs
Laser power (10 Hz)
Power (W)
XBL 799-2854

(Fig. 7)

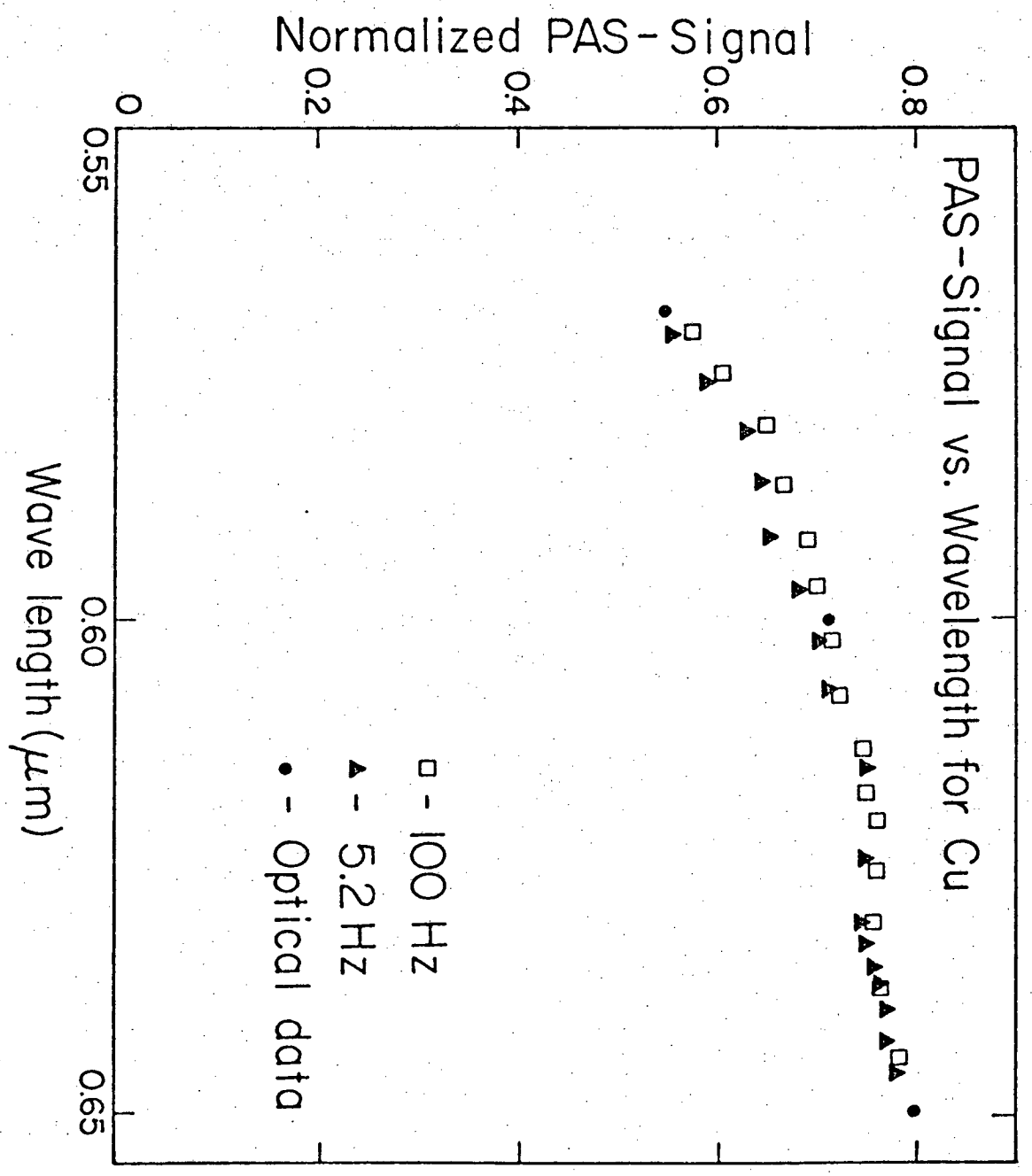
PAS-Signal vs. Wavelength for Cu
Normalized PAS-Signal
0
0.2
0.4
0.6
0.8
0.55
0.60
0.65
Wave length (μm)
□ - 100 Hz
▲ - 5.2 Hz
• - Optical data
XBL799-2852

(Fig. 8)

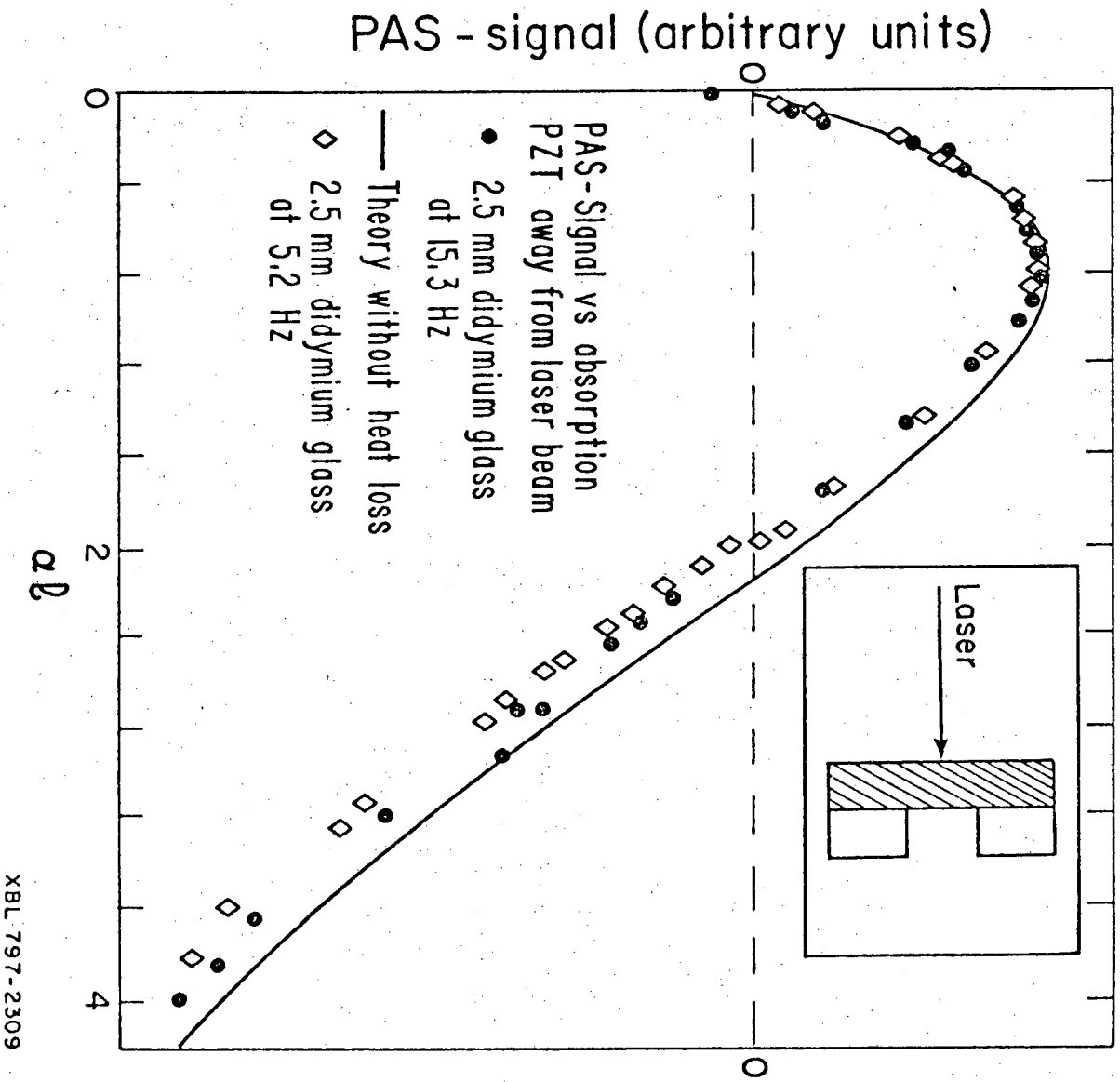
PAS - signal (arbitrary units)
PAS-Signal vs absorption
PZT away from laser beam
• 2.5 mm didymium glass
at 15,3 Hz
— Theory without heat loss
◇ 2.5 mm didymium glass
at 5,2 Hz
Laser
0
2
4
αl
XBL 797-2309

(Fig. 9)

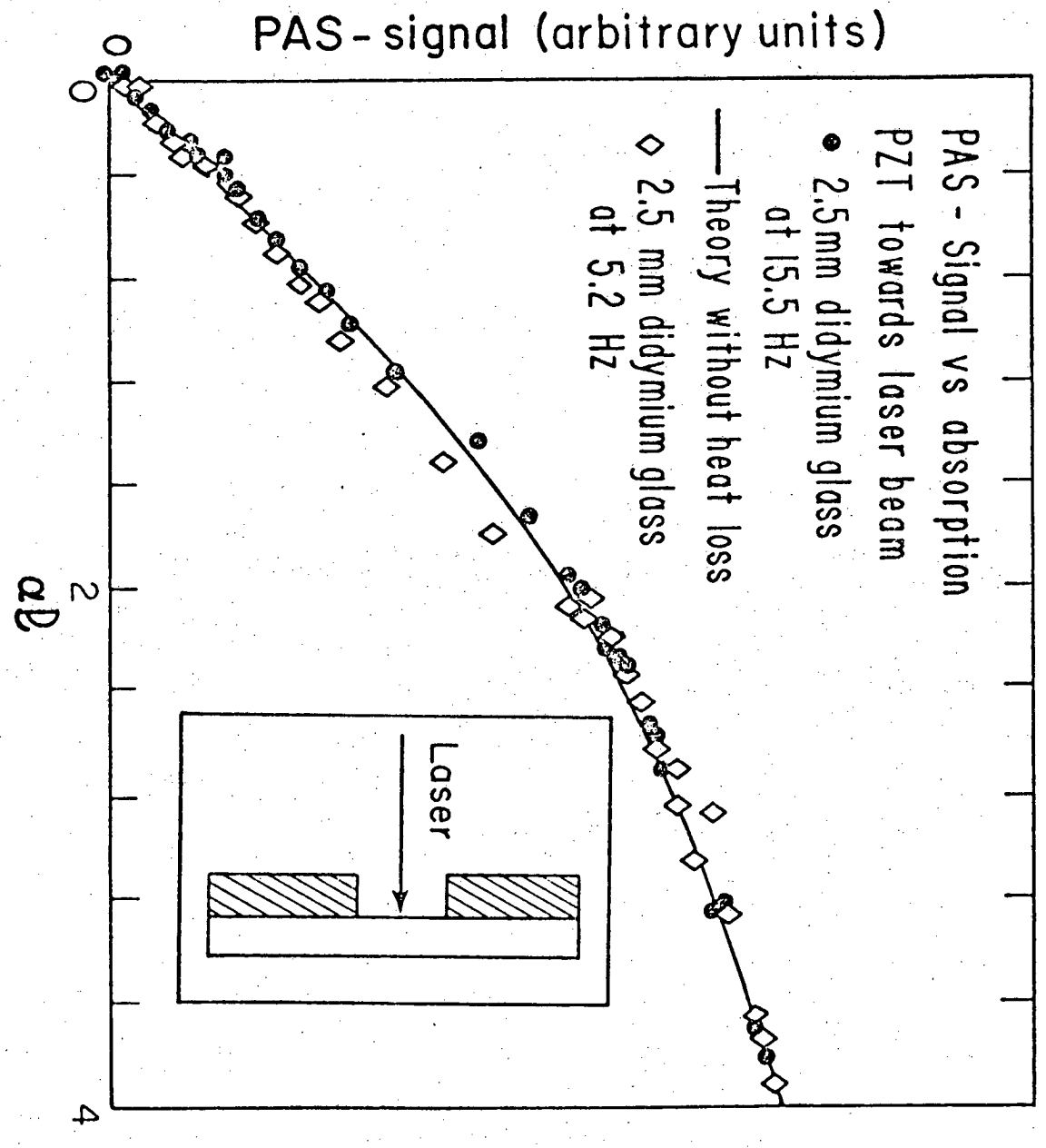

XBL 797-2308

(Fig. 10)

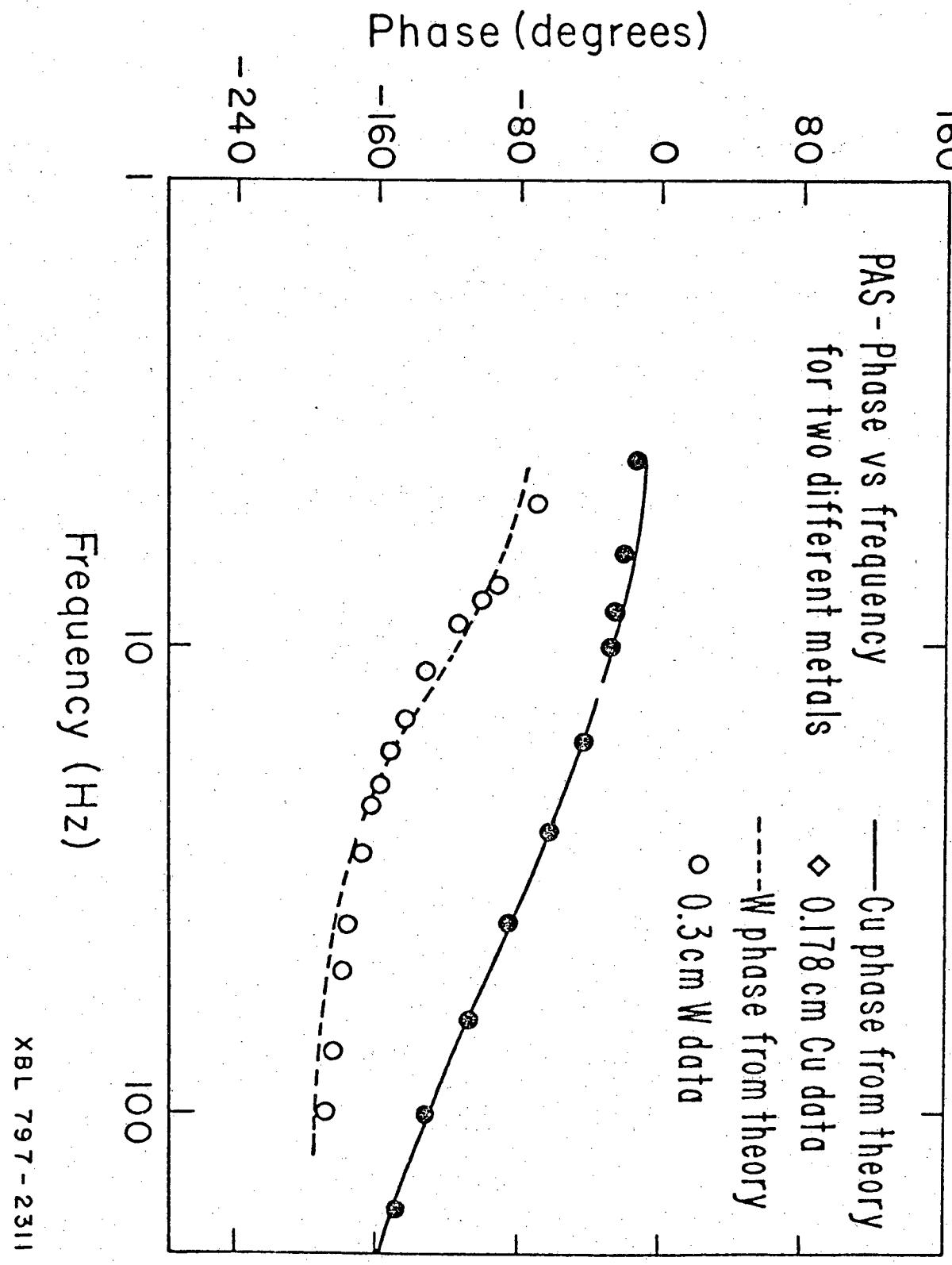
Phase (degrees)
160
80
0
-80
-160
-240
1
10
100
Frequency (Hz)
PAS - Phase vs frequency
for two different metals
——Cu phase from theory
◇ 0.178 cm Cu data
----W phase from theory
○ 0.3cm W data
XBL 797-2311

(Fig.11)

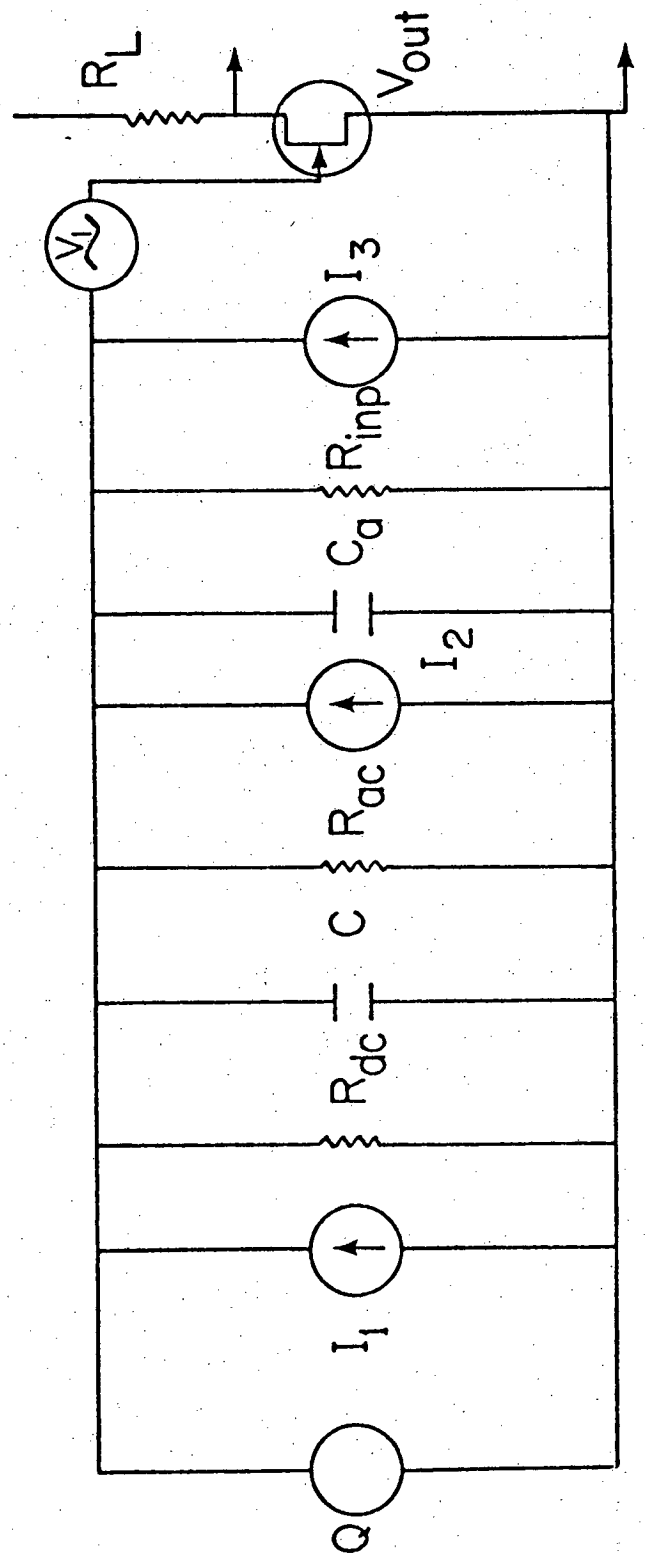

XBL 799-2853

Fig. (12)

COORDINATE GEOMETRY AND IDEALIZED MODE FOR STRESS CALCULATION

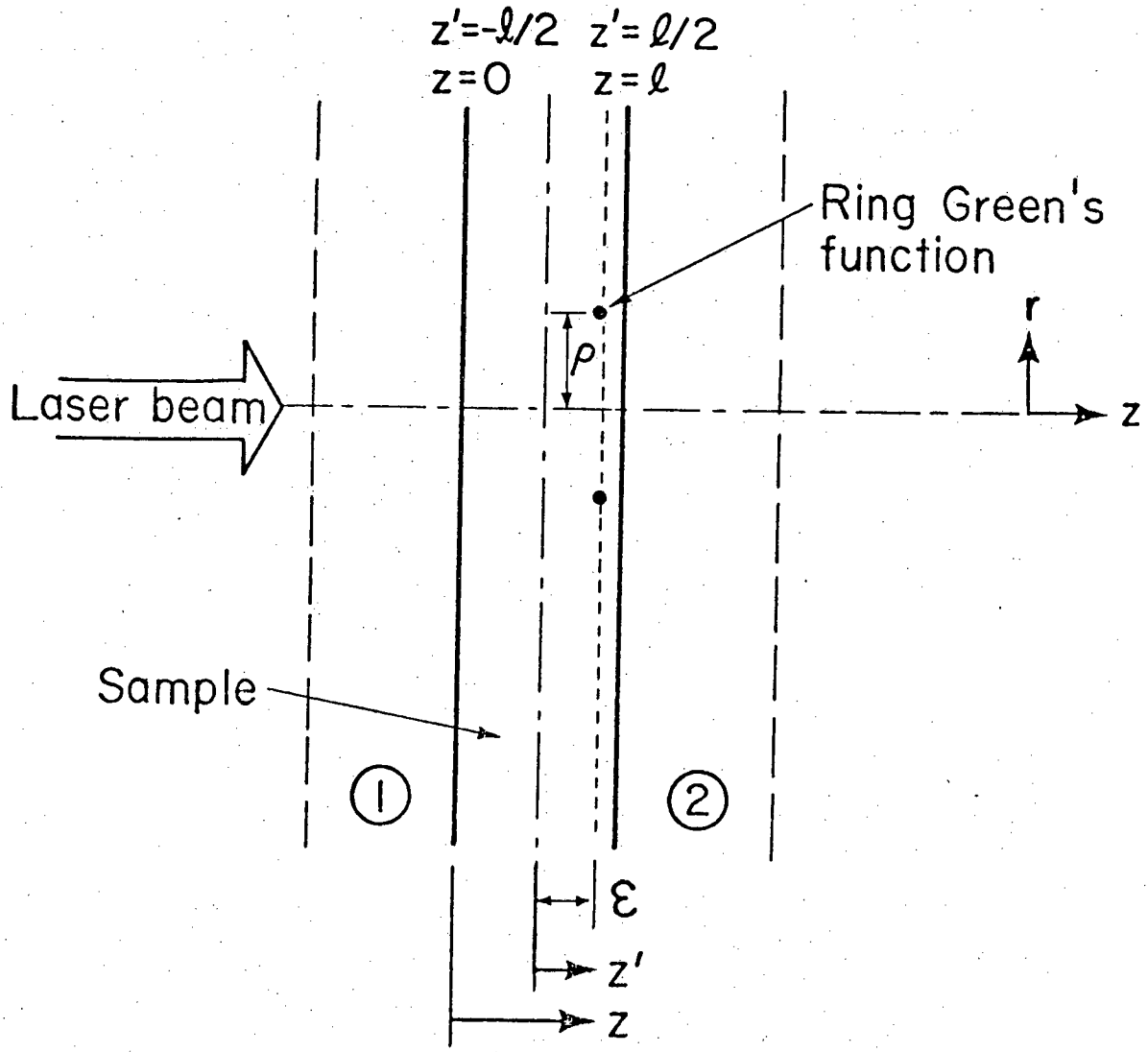

XBL 797-2314

(Fig.13)

This report was done with support from the Department of Energy. Any conclusions or opinions expressed in this report represent solely those of the author(s) and not necessarily those of The Regents of the University of California, the Lawrence Berkeley Laboratory or the Department of Energy.

Reference to a company or product name does not imply approval or recommendation of the product by the University of California or the U.S. Department of Energy to the exclusion of others that may be suitable.

TECHNICAL INFORMATION DEPARTMENT
LAWRENCE BERKELEY LABORATORY
UNIVERSITY OF CALIFORNIA
BERKELEY, CALIFORNIA 94720